

**Forschungszentrum Karlsruhe**  
Technik und Umwelt

**Wissenschaftliche Berichte**  
FZKA 5920

**Simulation Experiments  
on the Spreading Behaviour  
of Core Melts: KATS-5  
(1-dim spreading of an oxidic  
melt into a dry channel)**

**G. Fieg, H. Werle, F. Huber**

Institut für Neutronenphysik und Reaktortechnik  
Institut für Reaktorsicherheit  
Projekt Nukleare Sicherheitsforschung

Juni 1997

---



Forschungszentrum Karlsruhe  
Technik und Umwelt

Wissenschaftliche Berichte

FZKA 5920

Simulation Experiments on the Spreading Behaviour of Core  
Melts: KATS-5 (1-dim spreading of an oxidic melt into a dry  
channel)

G. Fieg, H. Werle, F Huber

Institut für Neutronenphysik und Reaktortechnik  
Institut für Reaktorsicherheit  
Projekt Nukleare Sicherheitsforschung

Forschungszentrum Karlsruhe GmbH, Karlsruhe  
1997

Als Manuskript gedruckt  
Für diesen Bericht behalten wir uns alle Rechte vor

Forschungszentrum Karlsruhe GmbH  
Postfach 3640, 76021 Karlsruhe

ISSN 0947-8620

## ABSTRACT

In future Light Water Reactors special devices (core catchers) might be required to prevent containment failure by basement erosion after reactor pressure vessel meltthrough during a core meltdown accident. Quick freezing of the molten core masses is desirable to reduce release of radioactivity.

Several concepts of core catcher devices, especially also for the EPR (European Pressurized Reactor) have been proposed based on the spreading of corium melt onto flat surfaces with subsequent water cooling. Therefore a series of experiments to investigate high temperature melt spreading on flat surfaces has been carried out using alumina-iron thermite melts as a simulant. The oxidic and metallic phases of the melt are separated and spread on different surfaces. The influence of a shallow water layer on the surface onto the spreading behaviour has also been studied.

In the KATS-5 experiment the spreading of an oxidic melt into a one-dimensional dry channel has been investigated. As to the metallic iron melt, the emphasis has not been on the spreading phase, but rather on the following flooding of the melt surface with water. This flooding test will be described in a separate report which will deal with further tests of this special objective.

## Simulationsexperimente zum Ausbreitungsverhalten von Kernschmelzen: KATS-5 (1-dim Ausbreiten einer oxidischen Schmelze in einen trockenen Kanal)

### ZUSAMMENFASSUNG

Für zukünftige Leichtwasserreaktor-Kraftwerke werden spezielle Einbauten (Kernfänger) erforderlich sein, um das Containment-Versagen infolge von Erosion des Fundamentes bei einem Kernschmelzunfall zu verhindern. Die geschmolzenen Kernmassen sollen möglichst schnell in einen festen Zustand übergeführt werden, um die Freisetzung von radioaktivem Material zu reduzieren.

Einige der vorgeschlagenen Kernfängerkonzepte, insbesondere auch für den EPR (European Pressurized Reactor), beruhen auf dem Prinzip, die geschmolzenen Kernmassen auf ebenen Flächen zu verteilen und anschließend mit Wasser zu kühlen. Es wurde deshalb eine Serie von Experimenten durchgeführt, um das Ausbreiten von Schmelzen mit hoher Temperatur auf ebenen Flächen zu untersuchen. Dabei wurde als Simulationsmaterial eine Thermitschmelze aus Aluminiumoxid und Eisen verwendet. Die oxidischen und metallischen Komponenten werden dabei getrennt und auf verschiedene Ausbreitungsflächen geleitet. Der Einfluß niedriger Wasserschichten auf den Flächen auf den Ausbreitungsprozeß wurde ebenfalls untersucht.

In KATS-5 wurde die Ausbreitung einer oxidischen Schmelze in einen eindimensionalen trockenen Kanal untersucht. Was die metallische Eisenschmelze betrifft, so lag das Interesse nicht am Ausbreitungsverhalten, sondern am nachfolgenden Fluten der Schmelzenoberfläche mit Wasser. Dieser Test wird in einem späteren Bericht beschrieben werden, der sich mit weiteren Flutungs-Tests beschäftigen wird.

CONTENTS	Page
1. Introduction	3
2. Experimental Setup	4
2.1 Test facility and thermite reaction	4
2.2 Instrumentation and data recording	6
2.3 Control system	7
3. Experimental conditions	7
4. Results	7
5. Summary	9
6. References	9

## 1. INTRODUCTION

Special devices (core catchers) might be required in future Light Water Reactors to prevent containment failure by basement erosion after reactor pressure vessel meltthrough during a core meltdown accident. It is desirable to cool, preferably freeze, the molten core masses quickly in order to reduce the release of radioactivity and the danger of interaction of the melt with structural materials. This implies that thin layers of corium are formed on these structures. Several concepts of core catchers have been proposed to meet these requirements [1-4].

Also the core catcher foreseen for the European Pressurized Reactor (EPR) is based on these principles [5,6], fig.1. The basic concept of this device is to retain the corium masses in the cavern under the reactor pressure vessel long enough to collect most of the corium inventory after the breach of the pressure vessel. Afterwards a gate opens between the cavern and a spreading compartment, into which the corium melt is released. This gate opens as a result of erosion by the melt and the time period for this process has to be about one hour, which is long enough to gather most of the corium after the breach of the pressure vessel. This time period will also allow an increase of the melt temperature and correspondingly a decrease of viscosity to assure a fast spreading of the melt. The composition of the corium is 180 tons of oxidic melt ( $\text{UO}_2$  and  $\text{ZrO}_2$ ) and 120 tons of metallic melt (steel and Zr). Cooling of the melt is foreseen from the top by flooding the melt surface with water after the end of the spreading phase.

Corium melt spreading and subsequent interaction of spread corium with water during flooding are generic problems of the EPR core catcher and similar concepts. Models are under development to describe these phenomena. They have to be verified by experiments. The number of experiments with real molten corium will be limited; therefore, tests with appropriate simulant materials are required.

The spreading of corium onto concrete floors has been investigated theoretically [7,8]. In addition, Susuki et al. [8] conducted several spreading experiments using stainless steel melts to verify their modeling. Moody [9] modeled the spreading of corium melt onto a flat surface with and without overlying water. The MELTSPREAD-1 code [10] has been developed at the Argonne National Laboratory and describes the spreading of melts onto dry and wet surfaces. Malinovic et. al. [11] investigated spreading of thermite melts on dry and wet concrete surfaces and also studied the quenching rates due to overlying water pools. Greene et. al. [12] studied the spreading of a variety of materials onto wet and dry surfaces to derive correlations for spreading rates and lengths.

At Siemens/KWU the CORFLOW code [13] has been developed for EPR core catcher investigations. This code describes the spreading of melts onto dry surfaces and has been verified by low temperature melt spreading experiments at the CORINE facility [13]. In addition, CORFLOW has to be verified with spreading experiments using higher temperature melts, and this is the main motivation for this series of experiments.

These tests are called KATS-experiments (abbreviation for Karlsruher Ausbreitungsexperimente mit Thermit-Schmelzen, Karlsruhe spreading experiments with thermite melts). Spreading experiments of separated alumina and iron melts on dry surfaces cannot directly simulate the spreading of real corium melts. The goal of these experiments is not to simulate as close as possible the behaviour of a corium melt, but to provide experimental data to validate CORFLOW. Therefore there is no need for a realistic scaling-up of the experimental layout to meet the EPR corecatcher design features. Knowledge of material properties, especially viscosity, for both, the simulant and the real melts is essential for extrapolating the results to reactor conditions using a computer model.

In this report the spreading of an oxidic melt into a one-dimensional dry channel is discussed. As to the metallic iron melt, the emphasis has not been on the spreading phase, but rather on the following flooding of the melt surface with water. This flooding test will be described in a separate report which will deal with further tests of this special objective.

## 2. EXPERIMENTAL SETUP

### 2.1 Test facility and thermite reaction

. The test rig, fig.2, consists of a large reaction crucible for thermite to generate molten alumina and iron, two containers under the crucible to gather the separated melts and the spreading areas (channels). To avoid thermal attack the crucible wall consists of a ceramic material (mainly magnesia). Fig.3 shows schematically the setup. The thermite powder (300 kg) in the crucible is heated up to 130 to 180 °C for about 24 hours before ignition to release any moisture. Thermocouples inside the thermite powder and the crucible wall control this heating-up phase. At the bottom of the crucible a nozzle, 40 mm in diameter, is installed to discharge the melt. The opening of the nozzle is performed by a pneumatic device, which is initiated by a central control unit. The thermite powder is ignited electrically at the top center of the load. The

reaction time for a 300 kg load lasts about 30 s. A delay time of 10 to 15 s between the end of the thermite reaction and the release is needed to allow outgassing of the melt. The arrival of melt at the nozzle is detected by three thermocouples which are located above the nozzle.

The specific energy of the exothermic thermite reaction  $8\text{Al} + 3\text{Fe}_3\text{O}_4 \rightarrow 4\text{Al}_2\text{O}_3 + 9\text{Fe}$  is  $3.85 \cdot 10^6$  J/kg, yielding an adiabatic melt temperature of 2600 °C. From experience it is known that only 95% of the thermite masses are reacting which reduces the melt temperature to 2450 °C. Due to wall erosion in the crucible and heat losses the temperature at the time of melt release is furthermore reduced to  $2200 \pm 50$  °C. This temperature has been calculated with the EquiTherm-Program [14]. It agrees well with measured values from temperature measurements of the jet (pyrometric method and with W/Re-thermocouples).

A load of 300 kg thermite produces 160 kg iron and 140 kg oxidic melt. The two phases of the melt, oxide and metal, separate practically immediately during the reaction and the iron melt pours firstly out of the nozzle after opening. The metallic and oxidic melts are gathered in two separate containers before spreading into the channels is initiated. The iron melt container is positioned under the nozzle outlet. Under the chosen experimental conditions the pouring takes about 8 s for the iron melt. Once the metallic melt is exhausted, the jet is guided into the second container by a movable chute. The containers are insulated with cordierite plates (52% SiO<sub>2</sub>, 37% Al<sub>2</sub>O<sub>3</sub>, 6.5% MgO) with an open porosity of 23%. This material is highly resistant to temperature shocks and erosion due to high temperature melt jets. Some wall material of both containers is dissolved into the melts because of the low melt temperature of cordierite (1600 °C). Due to incomplete thermite reaction and wall erosion the composition of the oxidic melt is more complicated. This will be discussed in detail in chapter 4. With the GEMINI-code [15] the solidus- and liquidus-temperatures of a mixture of oxides similar to this have been calculated, fig. 4. The liquidus-temperature is 1925 °C, in good agreement with experimental data from Elyutin et. al. [16].

The quality of separation of the two melt phases depends strongly on the time, when the jet is guided from the iron container into the oxide container via the movable chute. The time to move the chute is calculated under the assumption that the nozzle diameter does not increase due to material erosion. Furthermore, for a short time interval a mixture of oxidic and metallic melt may flow through the nozzle. Therefore a complete separation is not possible with this method. In the case that the jet is directed too late into the oxidic container some oxidic melt is gathered in the container for the iron melt. Except for the small resulting higher

pressure head in the container the spreading of iron is not disturbed by the presence of this oxide. Yet, in the case that the jet is directed too early into the oxide container, some iron gathers at the bottom of the oxide container and spreads onto the surface together with the oxide melt. To minimize this risk a "swamp" volume of more than 7 liters (equivalent to more than 40 kg of iron) for this excess iron melt in the oxide container has been foreseen, fig.5.

The gate between the oxide container and the spreading channel was closed with ceramic plugs made of magnesia. It is of a conical form with the smaller dimensions towards the container holding the melt, fig.5. The reason for this conical form is to insure a safe opening at the moment when the plugs are released by a pneumatic and mechanical spring device. The gate dimensions are: height 5 cm, width 34 cm. Figure 5 shows the dimensions of container, gate and spreading channel for the oxidic melt. The corresponding data are listed in Table 1. This table lists also the main parameters at the onset of spreading.

The spreading channel is constructed of concrete covered with cordierite plates and atop of the cordierite additionally with ceramic tiles having a water-tight surface (an alumina/silica mixture) as in the preceding tests KATS-3b and -4 [17]. The spreading channel has been adjusted carefully with a slope of less than 1mm over a length of 1 m against the horizontal. The channel length of 11.5 m has been chosen long enough to ensure that the oxide melt stops spreading before reaching the end of the channel.

## 2.2 Instrumentation and Data Recording

During the spreading process the temperature of the melts is measured with W-Re thermocouples at four different axial positions in the channel, with the thermocouple junction level 10 mm above the channel floor. Thermocouples of type K (1 mm outer diameter) are positioned at different vertical (5, 25, 45 mm above the floor level) and axial positions in the channel, table 2. These thermocouples have been installed to indicate the arrival time of the melt. Fig. 6 shows the positions and identification of the single measuring points. Several video-cameras record the spreading process.

The measured and amplified signals were recorded using a digital 32 channel transient recording system. A sampling rate of 1kHz per channel was applied leading to an overall recording time of 256 s. The transient recorder was started with the command to ignite the thermite powder. After conduct of the experiment the recorded data were transferred and stored on a disk. The evaluation is done with a special computer program supplied together with the transient

recorder system. For synchronisation reasons of the different video recorders, flashlights were triggered together with the commands for thermite ignition and opening of the gates.

## 2.3 Control System

The commands during conduct of the tests (thermite ignition, tapping the crucible orifice, moving the chute and opening the gates) are controlled by an electronic control system. The duration for the thermite reaction and hence the tapping of the orifice has been estimated with an established rule of thumb: the reaction front velocity proceeds at 25 to 30 mm/s for the thermite powder as used in these tests. The time intervals for the iron and oxidic melt to flow out of the reaction chamber have been calculated with Torricelli's law. From this, the time to move the chute leading the oxidic melt into the oxide container has been estimated. The opening of the gates are initiated after melt release from the reaction crucible was ended, Table 3 shows the timing of the different commands during conduct of the experiment.

## 3. EXPERIMENTAL CONDITIONS

Table 1 lists all relevant data at the onset of the experiment. Data of the post experimental analysis are also shown in this table. All metallic iron melt (25 kg) which has been accidentally poured into the oxide container, has been withheld from spreading due to the relatively large "swamp" volume.

The level of the oxide melt before opening the gate to the spreading channel can clearly be detected by post test analysis: up to the liquid level of 435 mm, fig. 5, the erosion of the cordierite wall was about 1-2 mm, there has been no erosion higher up in the container.

## 4. RESULTS

Fig. 7 shows traces of the W-Re thermocouples at three axial positions (0.3 m, 3.3 m and 6.3 m, measured from the gate). The oxide melt did not spread to the fourth type C thermocouple at 7.8 m. The maximum melt temperature close to the gate at 0.3 m is 2120 °C which is in rather good agreement with the calculated value of  $2177 \pm 50$  °C. Further downstreams the maximum temperatures are lower, 2050 °C at 3.3 m and 1670 °C at 6.3 m.

According to fig. 4 the temperature at 6.3 m is close to the solidus-point of 1577 °C. At this temperature the viscosity of the solid-liquid mixture is tremendously high compared to that of the pure liquid phase. One has to take into account that the response time of these relatively large C-type thermocouples is about 4 seconds. At the time when the thermocouple reading reached its asymptotic value, the oxide melt just arrived its final spreading. The low temperature at 6.3 m shows clearly that the spreading process is controlled by viscous forces. Table 4 shows the leading edge arrival times of the melt at the type K thermocouples locations. Included are also the average velocities as calculated from the thermocouple readings. Figs. 8 through 10 show the corresponding transient registrations for these thermocouples. Fig. 11 shows the transient spreading of the oxide melt at three different vertical positions (5 mm, 25 mm and 45 mm). The response time of these thermocouples is about 50 ms. Any systematic errors due to this response are cancelled in evaluating leading edge velocities because time differences are used between two different thermocouple readings. This figure shows that the leading edge front is 45 mm or higher up to a distance of about 5 m, at 6.3 m only two thermocouples at 5 mm and 25 mm heights detect arrival of the melt.

The pouring rate can be calculated according to Torricelli's law including a pouring factor of 0.6 for the given geometry [18]. It starts with 29.7 l/s at the onset of opening the gate and decreases linearly to zero within 3.6 seconds. The transient spreading of the oxide melt can be analyzed with the videorecordings. Fig. 12 shows the result together with the K-type thermocouple readings. Included in this picture is also the calculated pouring rate through the gate. Fig. 13 shows the profile of the spread melt in the channel. In this figure is shown that 25 kg of iron melt have been gathered in the swamp volume of the container. Additionally, an amount of about 10 kg oxide are found above this iron slug. This oxide was situated under the lower level of the gate opening and did therefore not pour through the gate. The height of the frozen oxide in the spreading channel is about 25 mm, averaged over the whole spreading length. The local height varied between 20 and 30 mm. The porosities of different probes in the spreading channel have also been analyzed and amount to ~25% in the average. This pretty high value is due to degassing of the spreading surface: on the spreading floor the gaps between the ceramic tiles have been closed with a cement, which degassed appreciably at the contact with the melt.

At several positions probes of the oxide have been taken and analyzed. Tab.5 shows the result of this SEM analysis at two positions, one inside the oxide container and the second one at 7 m

in the channel. The higher contents of MgO and SiO<sub>2</sub> in the container probe is due to the long period of cordierite wall erosion in the container. The composition of the mixture at 7 m distance is the one which is characteristic for the spreading melt. Fig. 14 shows REM-pictures of the two probes, inside the container and at 7 m in the spreading channel. Both pictures show distinctively two phases, a darker one containing Al<sub>2</sub>O<sub>3</sub>, which is enclosed in a brighter matrix. This brighter phase (spinell) consists of SiO<sub>2</sub>, Al<sub>2</sub>O<sub>3</sub>, FeO, MgO and MnO. In agreement with the SEM analysis, the probe at 7 m shows a higher content of the darker phase (pure Al<sub>2</sub>O<sub>3</sub>) and the crystal structure is dendritic, which is due to the fast cooling rate during spreading.

## 5. SUMMARY

The one-dimensional spreading of an oxidic melt with an initial temperature of 2120 °C (liquidus 1925 °C, solidus 1577 °C) into a dry channel with a ceramic surface has been studied. The melt spread evenly over a distance of 7.5 m (average height of the frozen oxide about 25 mm). The measured melt temperature of 1670 °C in the final stage of spreading is far below the liquidus temperature, indicating that the spreading length is determined by viscous forces and possibly crust formation.

## 6. REFERENCES

1. J.D. Fish, M. Pilch and F. Arrellano, "Demonstration of Passively-Cooled Particle-Bed Core Retention," Proceedings of the 5<sup>th</sup> Post Accident Debris Cooling Information Exchange Meeting, Karlsruhe, Germany, 28-30 June 1982, 319-324
2. H. Alsmeyer et. al., "Improved Containment Concepts for Future Large LWR's," IEA Int. Conf. Technology Responses to Global Environmental Challenges, Kyoto, Japan, 6-8 November 1991, 471-489
3. A. Turricchia, "How to Avoid Molten Core/Concrete Interaction and Steam Explosions," Proc. 2nd Organization for Economic Cooperation and Development Committee on the Safety of Nuclear Installations Specialist's Meeting on Molten Core Debris-Concrete Interaction, Karlsruhe, Germany, April 1992, KfK-Report 5108, 503-518

4. J.M. Seiler, F. Balard, M. Durin, A. Méjane, S. Pigny and I. Szabo, "Conceptual Studies of Core Catchers for Advanced LWR's," Proc. Int. Conf. Design and Safety of Advanced Nuclear Power Plants, Tokyo, Japan, October 25-29, 1992, Vol III, p. 300-327
5. M. Michel et. al., "EPR Safety Approach and Consideration of Severe Accidents," Transactions of the ENC '94, Lyon, France, October 2-6, 1994, Vol.II, 502-506
6. M. Fischer, Siemens/KWU, private communication, May 1996
7. M.S. Kazimi, "On the Liner Failure Potential in MARK-I Boiling Reactors," Nucl. Science and Engineering, **103**, 59-69 (1989)
8. H. Suzuki, T. Mitadera, I. Sakaki and T. Zama, "Fundamental Experiment and Analysis for Melt Spreading on Concrete Floors," Proc. Intern. Conference on Nucl. Energy (ICONE-2), San Francisco, March 21-24, 1993
9. F.J. Moody, "First Order Analyses of Molten Corium Heat Transfer," ANS Proc. 1989 National Heat Transfer Conference, August 6-9, 1989, Philadelphia, PE, 217-224
10. M.T. Farmer, J.J. Sienicki, B.W. Spencer and C.C. Chen, "Status of the MELTSPREAD-1 Computer Code for the Analysis of Transient Spreading of Core Debris Melts," Proc. 2nd Organization for Economic Cooperation and Development Committee on the Safety of Nuclear Installations Specialist's Meeting on Molten Core Debris-Concrete Interaction, Karlsruhe, Germany, April 1992, KfK-Report 5108, 489-502
11. B. Malinovic and R. E. Henry, "Experiments Relating to Drywell Shell-Core Debris Interaction", EPRI-NP 7196L (February 1991)
12. G.A. Greene, K.R. Perkins and S.A. Hodge, "Mark I Containment Drywell-Impact of Core/Concrete Interactions on Containment Integrity and Failure of the Drywell Liner," Proceedings of an International Symposium on Source Term Evaluation for Accident Conditions, Columbus, OH, October 28-November 1, 1985, pp 429, International Atomic Energy Agency, Vienna, (1986).
13. J. M. Veteau and R. Wittmaack, "CORINE Experiments and Theoretical Modelling," FISA-95 Symposium - EU Research on Severe Accidents, Luxembourg, Nov. 20-22, 1995, 271-285

14. M. Steinbrück, private communication
15. M. Steinbrück, private communication
16. V.P. Elyutin et.al., "Viscosity of Alumina", Russian Journal of Physical Chemistry, 43(3), 1969, siehe auch: D.A. Powers, A.W. Frazier, "VISRHO, A Computer Subroutine for Estimating the Viscosity and Density of Complex Silicate Melts", SAND 76-0649, June 1977
17. G. Fieg, H. Werle, F. Huber, "Simulation Experiments on the Spreading Behaviour of Molten Core Melts: KATS-3b and KATS-4", FZKA 5587-Report, Forschungszentrum Karlsruhe, 1997
18. Dubbel Taschenbuch für den Maschinenbau, Springer Verlag, 17. Auflage, 1990, B52-B53

**Table 1 Dimensions of oxide melt container, spreading channel, melt height and mass for KATS-5**

	Unit	
Container inner width	cm	37.8
Container inner depth	cm	32.5
Release gate height	cm	5.0
Release gate width	cm	34.0
Channel width	cm	40.0
Channel length	m	11.5
Height of oxide melt <sup>2)</sup>	cm	43.5
Calculated oxide melt <sup>1)</sup>	kg	140.0
Actual oxide melt <sup>2)</sup>	kg	144.2

<sup>1)</sup> Data calculated under the assumption of ideal melt separation

<sup>2)</sup> Data derived from post experimental examination

**Table 2 Location of thermocouples in test KATS-5  
(oxide melt)**

Axial position of thermocouples (m)	Thermocouple #		
	Vertical positions of thermocouples		
	5 mm	25 mm	45 mm
0.3	O.TK.0305 O.TW.0305	O.TK.0325	-
1.8	O.TK.1805	O.TK.1825	O.TK.1845
3.3	O.TK.3305 O.TW.3305	O.TK.3325	O.TK.3345
4.8	O.TK.4805	O.TK.4825	O.TK.4845
6.3	O.TK.6305 O.TW.6305	O.TK.6325	O.TK.6345
7.8	O.TK.7805 O.TW.7805	O.TK.7825	O.TK.7845
9.3	O.TK.9305	O.TK.9325	O.TK.9345

TK= K-type thermocouple

TW= C-type thermocouple

**Table 3 Time charts of the KATS control system for test KATS-5 (oxide melt)**

KATS-5 (Oxide melt)	
Event	Time (s)
Ignition of thermite powder Flashlight #1 Start Videosystem	0
Start of melt release	45.0
Start of moving chute	53.0
Chute on end position	55.5
Open gate for oxide melt Flashlight #2	80.1

**Table 4** Arrival times and velocities of oxide melt at axial and vertical thermocouple locations in test KATS-5

Axial position of thermocouples (m)	Melt arrival times (s)		
	Melt velocity (m/s)		
	Vertical positions of thermocouples		
	5 mm	25 mm	45 mm
0.3	0.165s	0.19s	(no thermocouple)
	2.65 m/s	2.73 m/s	-
1.8	0.73s	0.74s	0.81s
	1.94 m/s	1.85 m/s	1.68 m/s
3.3	1.50s	1.55s	1.70s
	0.65 m/s	0.67 m/s	0.72 m/s
4.8	3.80s	3.79s	3.77s
	0.51 m/s	0.55 m/s	-
6.3	6.75s	6.5s	-
	-	-	-
7.8	-	-	-
	-	-	-
9.3	-	-	-

Melt front velocities between two consecutive axial thermocouple positions at identical vertical locations

**Table 5 SEM-Analysis of two oxidic KATS-5 samples**

	Sample Position	
	Container (wt %)	Spreading channel (7.0 m) (wt %)
MgO	4.3	1.5
Al <sub>2</sub> O <sub>3</sub>	80.2	86.1
SiO <sub>2</sub>	8.6	6.1
MnO	1.4	0.9
FeO	5.5	5.4

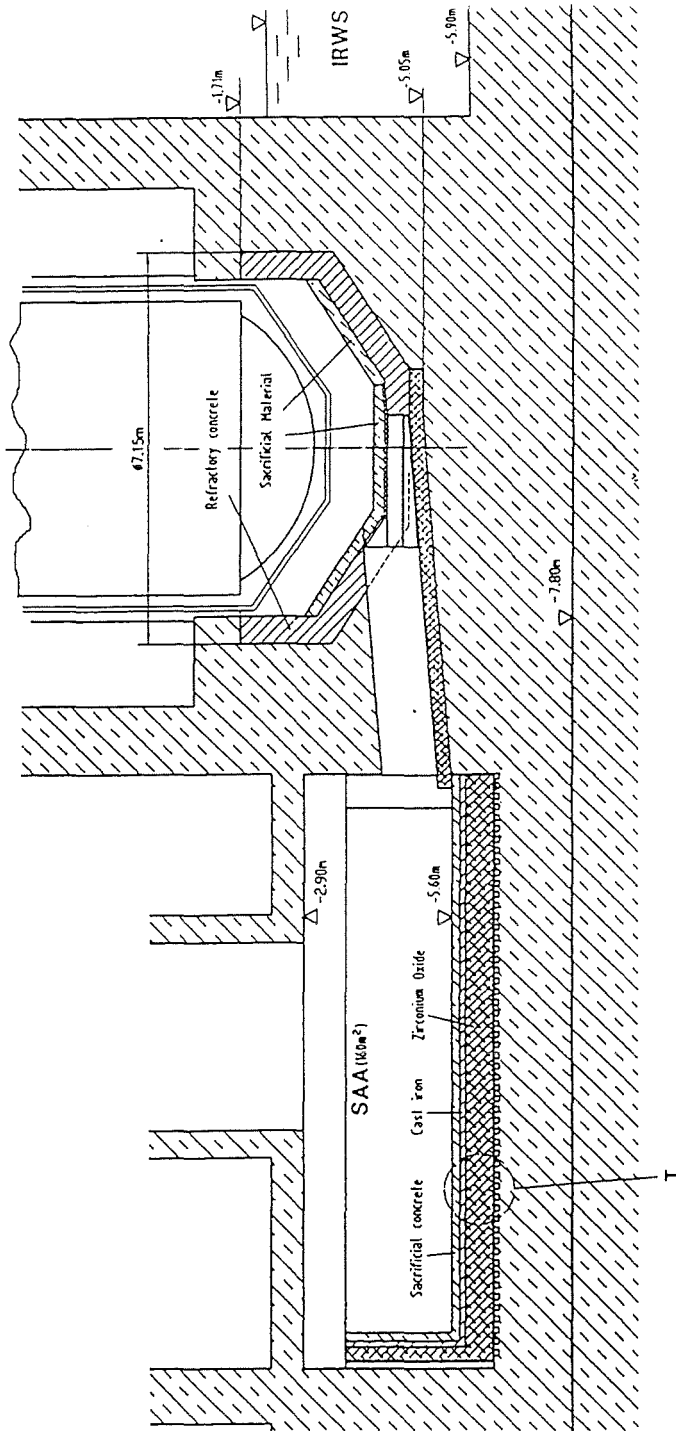
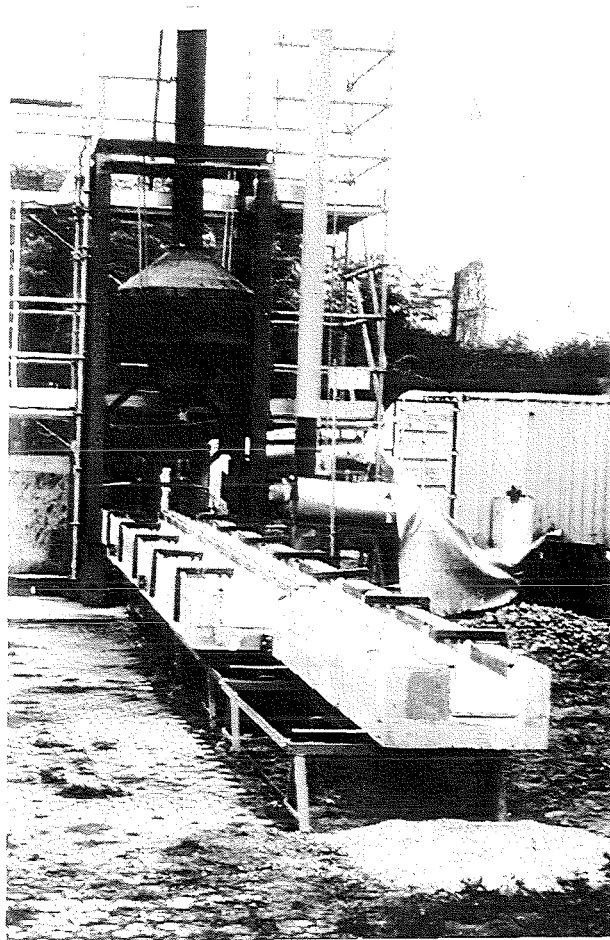
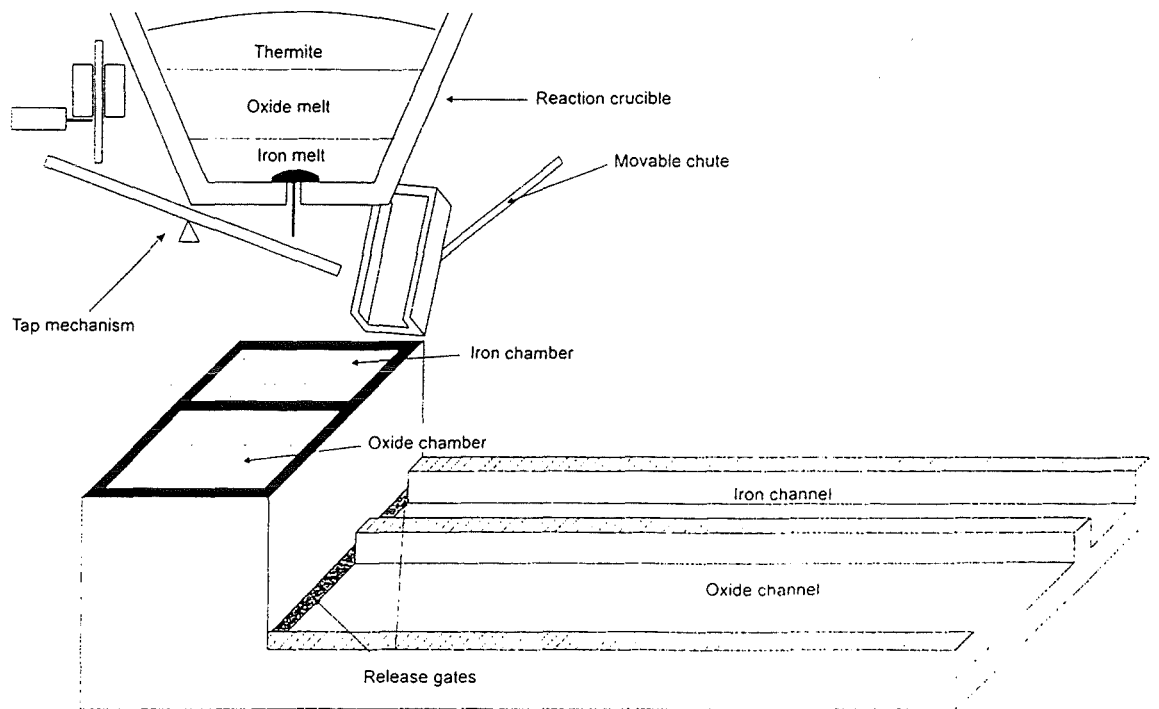


Fig. 1 Improved Reference Concept of the EPR  
Core-melt Retention System



**Fig.2 Photo of the KATS Facility**



**Fig.3 Schematics of the KATS Facility**

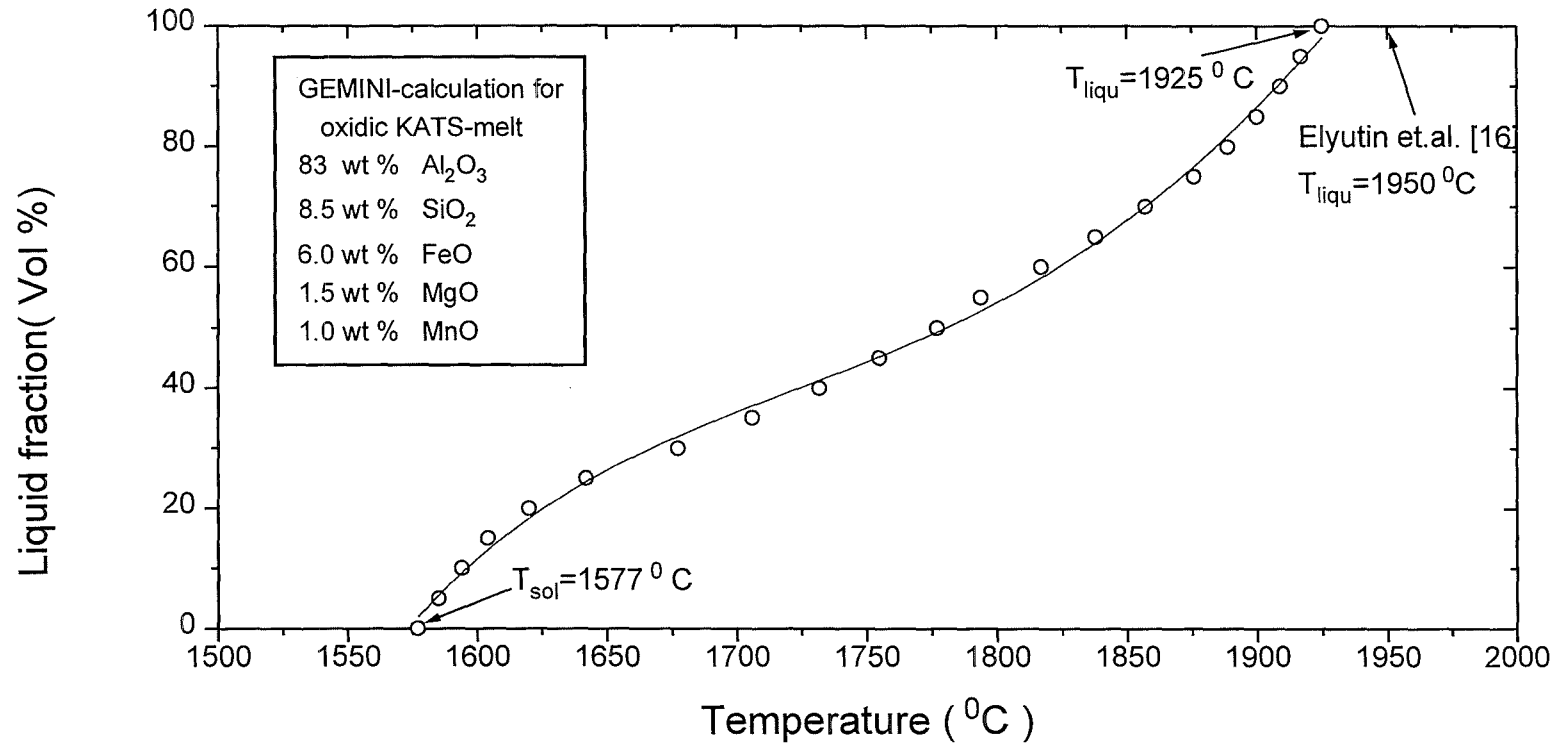
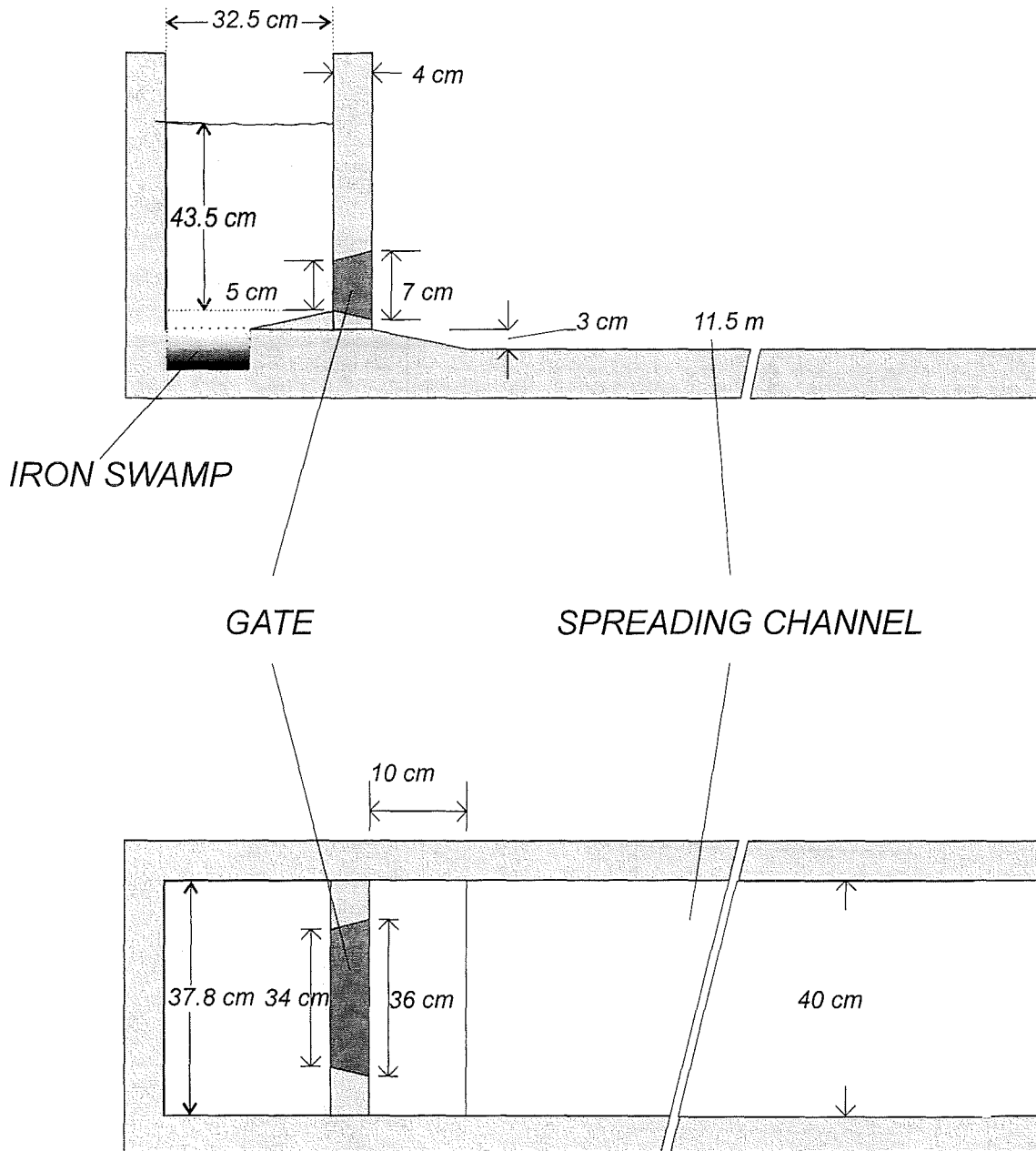
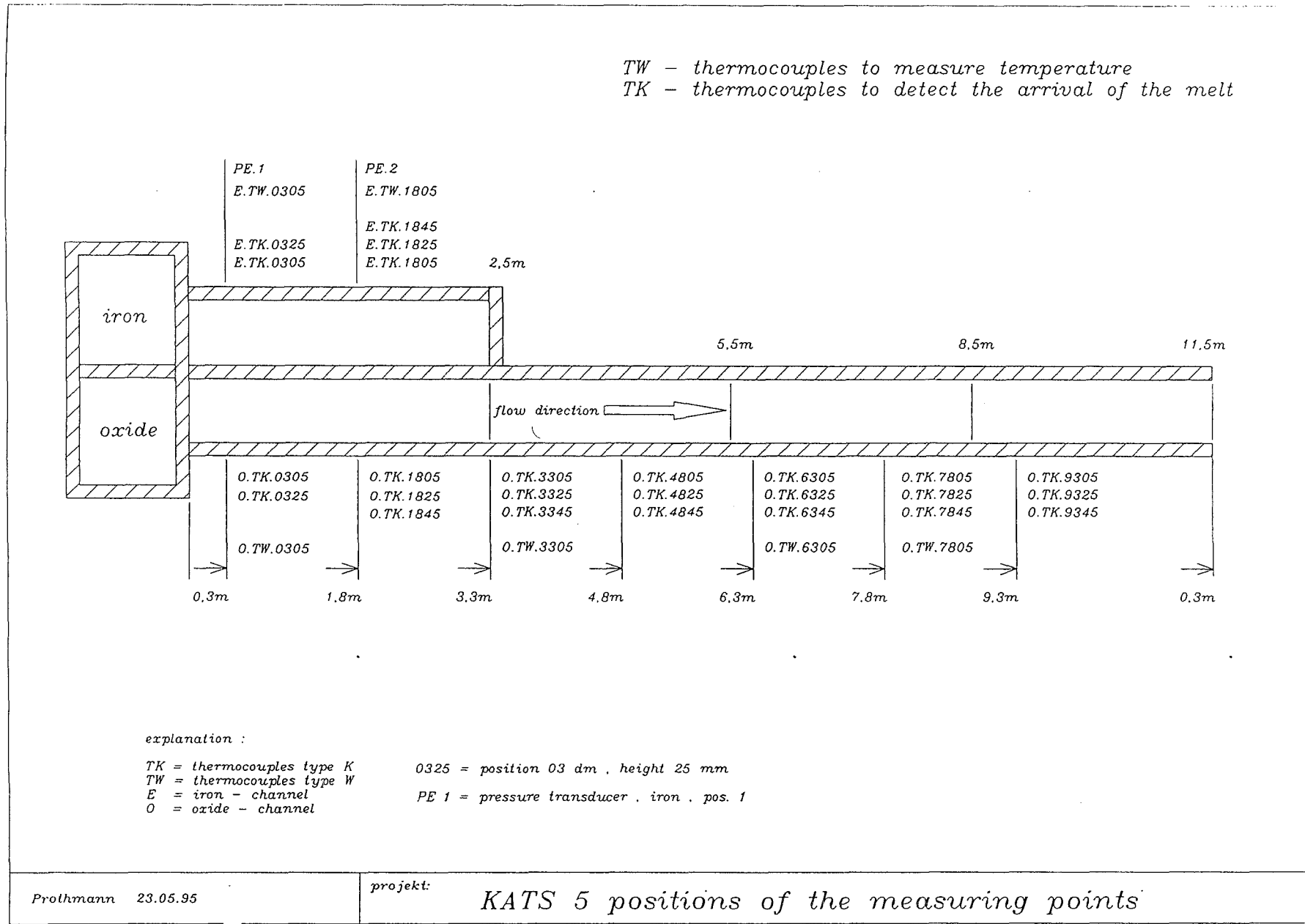


Fig. 4 Liquid fraction of an oxidic KATS melt between liquidus- and solidus-temperatures [15]



**Fig. 5 Geometry and dimensions for the spreading of oxide melt in KATS-5**

Fig.6 Test KATS-5, positions of thermocouples



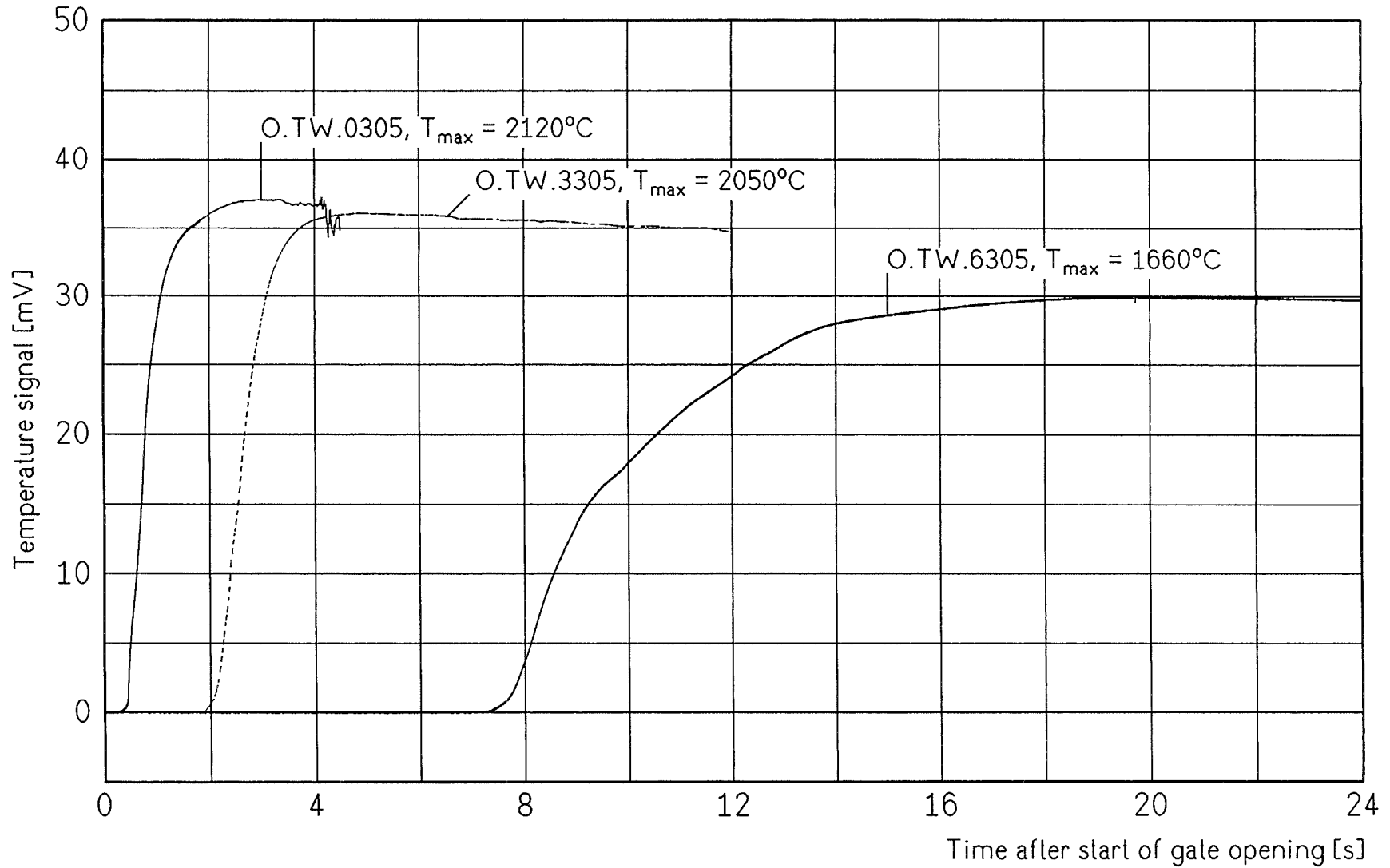


Fig.7 Test KATS-5 Temperature of the oxide melt at pos. 0.3/3.3/6.3m

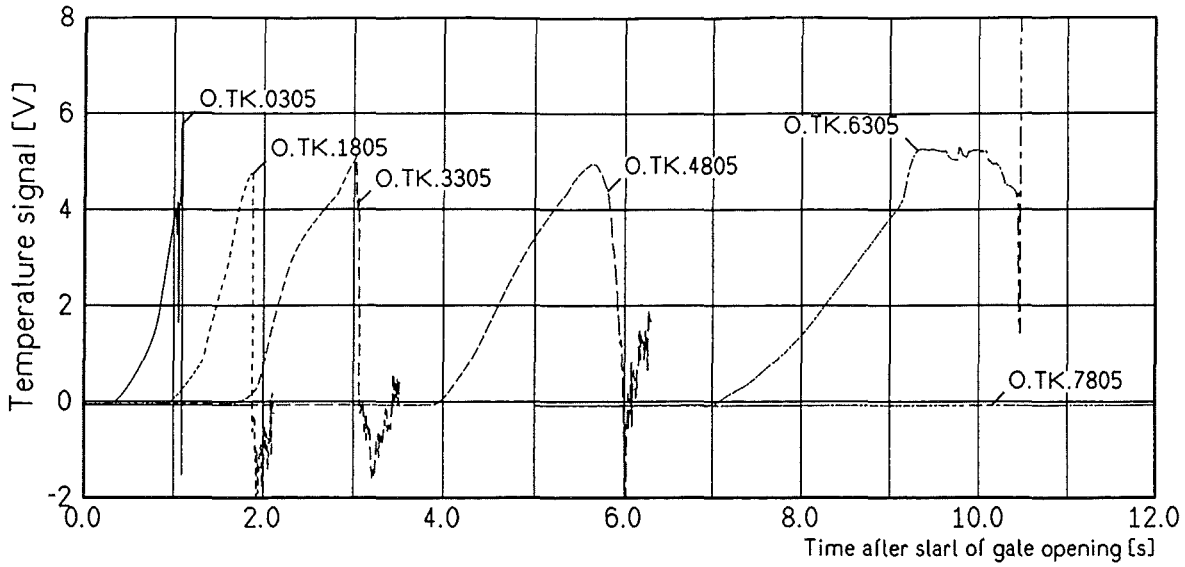


Fig. 8 Test KATS-5 Detection of the oxide melt at 5mm height

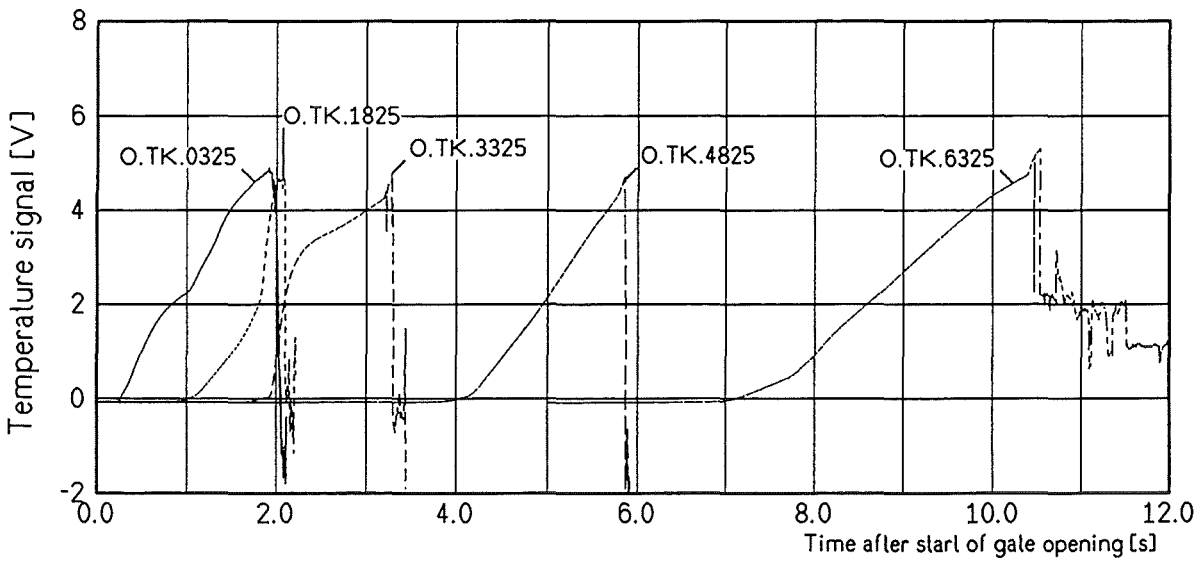


Fig. 9 Test KATS-5 Detection of the oxide melt at 25mm height

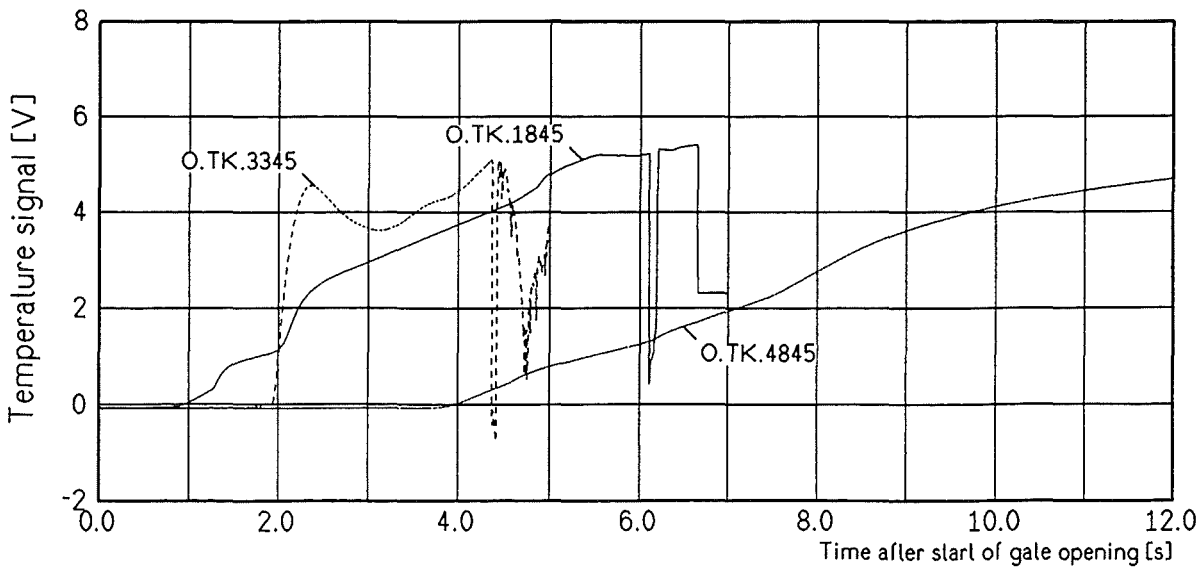


Fig. 10 Test KATS-5 Detection of the oxide melt at 45mm height

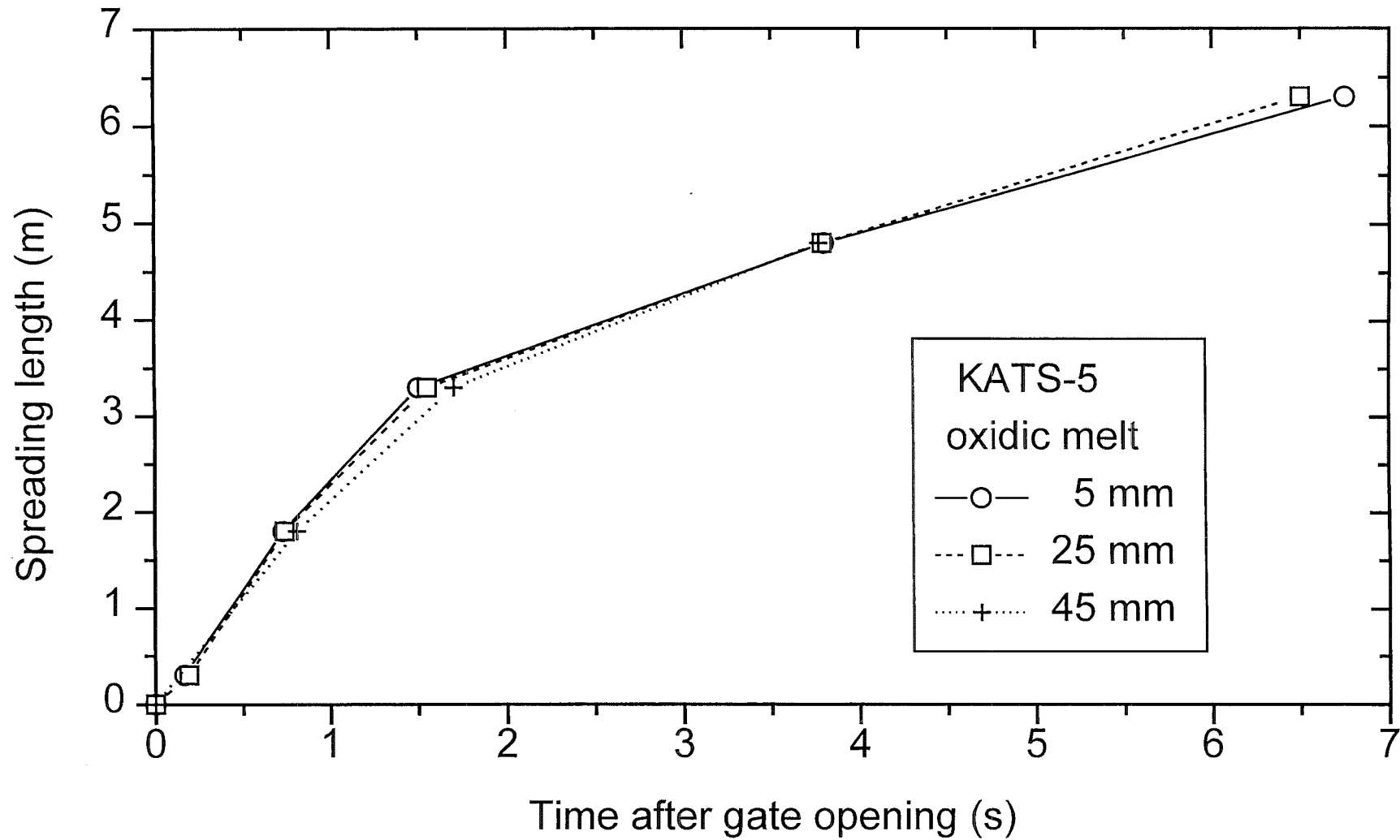


Fig. 11 Test KATS-5: Transient spreading of oxidic melt at different vertical positions

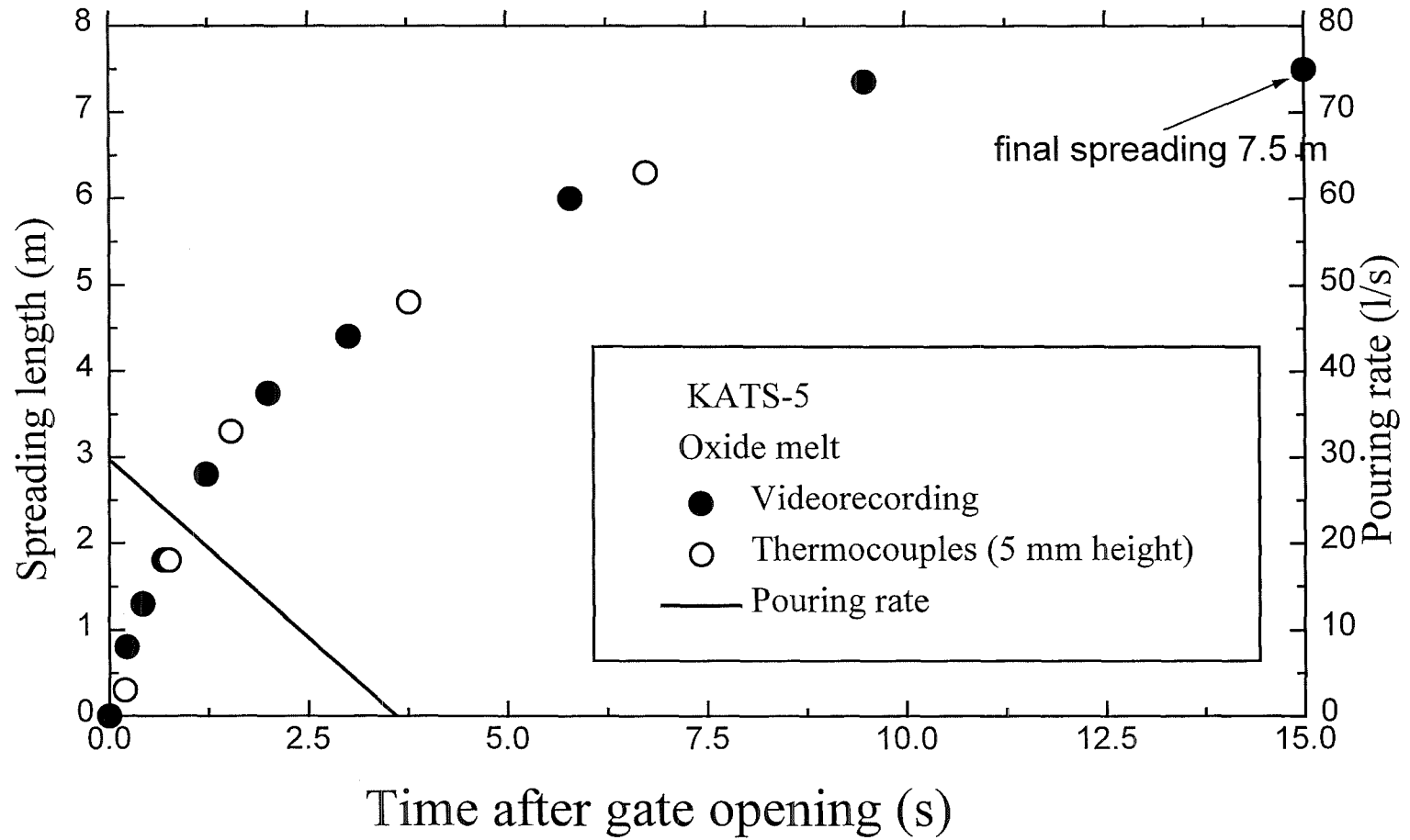


Fig. 12 Transient spreading of oxidic melt into channel

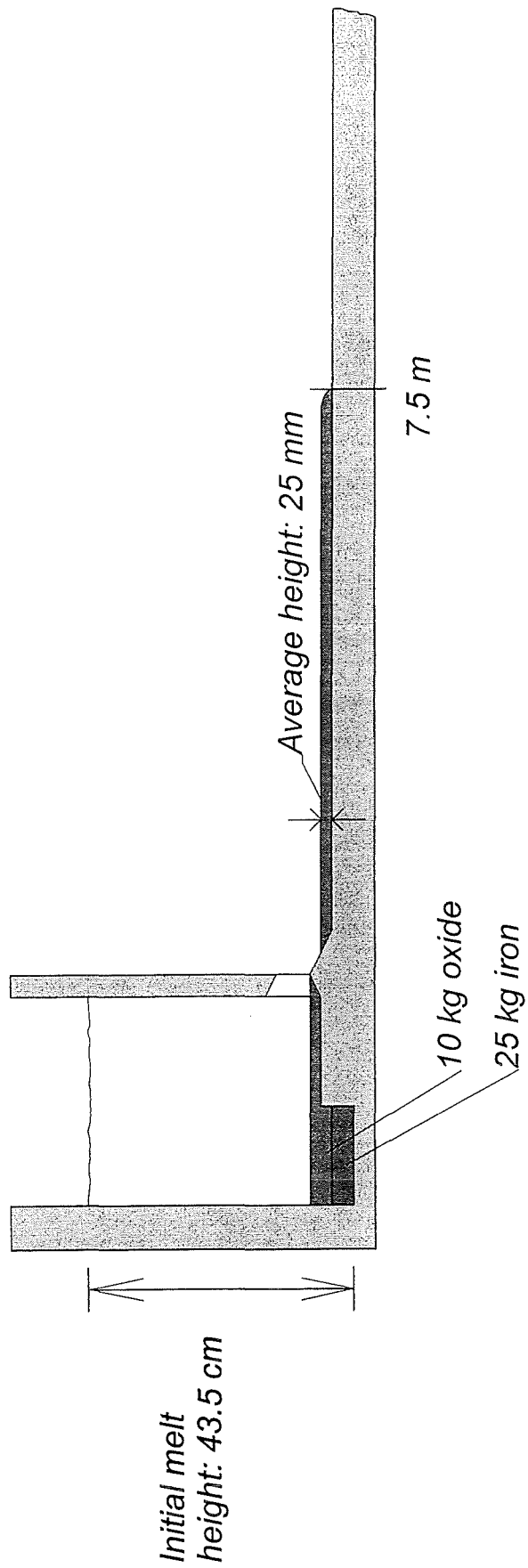


Fig.13 Post experiment distribution of the oxide melt in test KATS-5

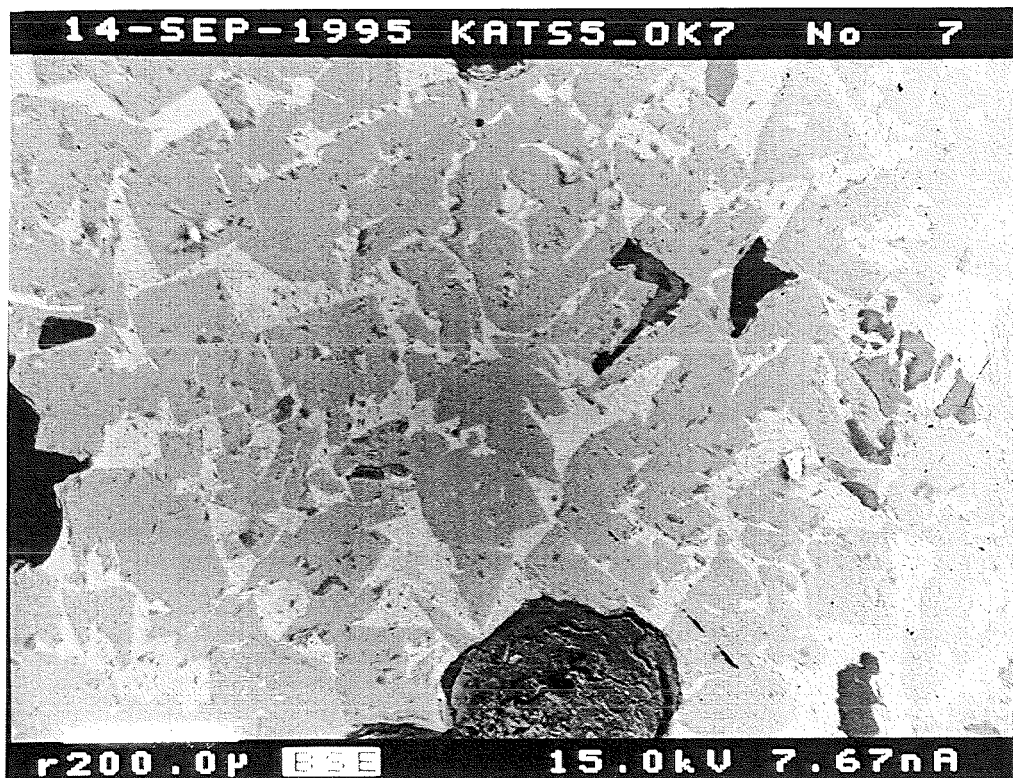


Fig.14 REM pictures of oxidic samples of test KATS-5  
Top: container Bottom: channel at 7 m